IEEE Access
Multidisciplinary | Rapid Review | Open Access Journal

Received August 3, 2020, accepted August 11, 2020, date of publication August 19, 2020, date of current version September 1, 2020.

Digital Object Identifier 10.1109/ACCESS.2020.3017773

Large-Scale Analysis of the Head Proximity Effects on Antenna Performance Using Machine Learning Based Models

YINLIANG DIAO[1,2], (Member, IEEE), ESSAM A. RASHED[1,3], (Senior Member, IEEE), AND AKIMASA HIRATA[1,4], (Fellow, IEEE)

[1]Department of Electrical and Mechanical Engineering, Nagoya Institute of Technology, Nagoya 466-8555, Japan
[2]College of Electronic Engineering, South China Agricultural University, Guangzhou 510642, China
[3]Department of Mathematics, Faculty of Science, Suez Canal University, Ismailia 41522, Egypt
[4]Center of Biomedical Physics and Information Technology, Nagoya Institute of Technology, Nagoya 466-8555, Japan

Corresponding author: Yinliang Diao (diaoyinliang@ieee.org)

This work was supported by Ministry of Internal Affairs and Communications Grant Number JPMI10001.

ABSTRACT Owing to the variations in subject-specific body morphology and anatomy, the radiation performance of a wireless device in the presence of human body is different across subjects. To quantify the inter-subject variations, a large number of highly realistic human models are required. One recent approach is the fast development of body models directly from medical images with machine learning. In this study, a total of eighteen anatomical head models were developed using a fast machine learning approach and were then adopted for large-scale evaluation of the inter-subject variations in antenna performance. The antenna impedance, return loss (RL), total radiated power (TRP), directivity, radiation patterns, and specific absorption rate (SAR) were investigated. The results show rather large variations in impedance, RL, and SAR across subjects, while TRP, directivity, and radiation pattern are less likely to be affected by internal tissue distributions when compared with homogeneous models.

INDEX TERMS Antenna performance, electromagnetic exposure, FDTD method, machine learning.

I. INTRODUCTION

In recent decades, the striking advances in wireless communication techniques have triggered various applications facilitating human daily lives [1]. Aside from general consumer electronics such as mobile phones, virtual display systems, smart watches, and headbands, there has been a trend toward using personalized wireless devices for healthcare applications, associated with the aging population increase [2]. It can be envisaged that multiple sensors/devices will be utilized on the human body to form a wireless network, which not only consists of wearable/implantable sensors, but also on-body gateways.

A robust antenna design is essential to achieve high integration, long battery life, and robust performance for wireless communication applications [3]. When operating in close proximity to the human body, the antenna performance is affected by the interaction with the human body, which behaves as a lossy dielectric. As the wireless link budget is tight, the radiation efficiency should be improved as much as possible, considering that the wireless signal transmission accounts for a large portion of the overall power consumption.

Characterization of the radiation performance will enable manufacturers to determine how appropriate the wireless devices will perform. In volunteer studies, user effects on mobile phone antennas have been investigated by measurements [4]–[6]. Reference [5] revealed a total radiated power (TRP) standard deviation (SD) approximately 0.4 dB for a mobile phone antenna operating at 1.8 GHz. In [6] and [7], substantial shadowing effect from the body was observed at 15 GHz and 28 GHz for 5G networks using millimeter-wave technology. However, it is difficult to fix the measurement condition, resulting in additional variability [8]. In addition, the specific absorption rate (SAR), which is the power deposition per unit mass, averaged over 10 g of tissues, cannot be measured in live humans.

In these circumstances, computational approaches are often used. To achieve an optimized design, detailed human

The associate editor coordinating the review of this manuscript and approving it for publication was Wen-Sheng Zhao.

models should be considered in the design process to accelerate the development and ease the tuning effort, especially for personalized wireless devices [9]. The coupling between the antenna and the human body has been studied by numerical methods [10]–[16] and voxel-based human body models. The development of anatomical voxel human models from medical images includes efforts for identifying and segmenting each tissue/organ. Commonly used models include the TARO and HANOKO models developed by NICT, Japan [17], Virtual population models developed by IT'IS foundation, Swiss [18], NORMAN [19], and NAOMI [20] developed by the NRPB, UK. In these models, the tissue-specific dielectric properties are uniformly assigned to each tissue. The automatic segmentation accuracy is still a challenging topic and in some tissues, its accuracy is limited to 80–90% in terms of dice coefficient [21].

Furthermore, the existing voxel-based human models were developed from magnetic resonance images (MRIs) of specific subjects; therefore, it is difficult to conduct group-level evaluation studies of wireless performance (or personalized optimization of wireless devices), which significantly depends on precise individual anatomical models [22]. Moreover, the number of available models is insufficient for inter-subject variation consideration. Furthermore, the dielectric properties are known to be subject-dependent; for example, the dielectric properties of children and elderly are different from those of adults due to different water content and ion concentration [23].

Another metric to be evaluated in antenna design is SAR. According to the international guidelines and standards of electromagnetic safety [24], [25], the peak spatial-average SAR (psSAR) that averaged over 10 g of tissue should be assessed. The limit in the head is 2 W/kg for the general public from 100 kHz to 6 GHz. For compliance assessment of product safety, a specific anthropomorphic mannequin (SAM) head phantom filled with homogeneous tissue equivalent liquid has been specified for psSAR measurements [26]. The same phantom was also adopted for the test of the over-the-air (OTA) performance [27]. The dielectric properties for OTA test are also directly adopted from those designed for the SAR compliance measurement, with the original intention of providing a slightly more conservative psSAR estimation [28]. Uncertainties in using homogenous SAM phantoms have been studied by comparing them with inhomogeneous anatomical models [29]–[32]. In addition, studies on antenna design with low SAR has been conducted widely [33]–[37]. However, these studies mainly focus on the electromagnetic absorption inside the human model, and few studies have been conducted on the subject-specific antenna radiation performance.

The appropriateness of using a homogenous tissue simulant liquid for performance evaluation of personalized wireless devices is unclear. Recently, machine learning based techniques have been adopted for estimation of tissue properties directly from medical images without tissue segmentation [38]–[41]. In [38], the brain tissue conductivities were derived from measured B1 map using a dictionary-based algorithm. Reference [39] proposed a global Maxell tomography for noninvasive estimation of electrical properties from MRI. A convolutional neural network architecture was proposed in [40] for automatic generation of head models with non-uniform tissue conductivities from T1 and T2 MRI scans, these models were then adopted for evaluation of the induced electric field in brain during transcranial magnetic stimulation. In general, the machine learning based modeling techniques allow fast generation of subject-specific body models, which can be utilized for estimation of electromagnetic exposure doses, improvements of brain stimulation apparatus [40] and radio-frequency therapeutic applications [42]. In our previous work [41], eight head models were developed from MRIs using a deep learning approach with network architecture (known as CondNet) without tissue segmentation because of image-based dielectric property assignment, and were successfully used for numerical dosimetry assessments. The feature of this approach is that tissue-specific conductivity assignment is not required. Thus, a smooth distribution of dielectric properties and tissue densities can be provided. However, in that study, we only considered the electromagnetic deposition in the exposed heads. The applicability of the learning-based models for evaluation of the antenna-body mutual coupling has not been thoroughly examined yet. Also, the limited number of models used in that study is not enough to formulate a robust statistical analysis.

In this study, CondNet is used to develop eighteen head models from MRIs, hence permitting a large-scale analysis of the effects on antenna performance due to head proximity. The antenna radiation performances are evaluated in these models using the finite-difference time-domain (FDTD) method [43]. The effects of inter-subject variations on the antenna impedance, return loss (RL), TRP, directivity, radiation patterns, and psSAR were comprehensively investigated for the first time. Head models with homogeneous dielectric properties were also adopted to distinguish the uncertainties caused by the homogeneity of the tissue properties and the outer head geometry. The remainder of this article is structured as follows. Section II describes the machine learning approach for the development of head models and the electromagnetic simulation method. In Section III, we first present the results calculated using the eighteen head models with homogeneous dielectric properties, and then the results using learning-based head models with in-homogeneously distributed dielectric properties, followed by a comparison with segmented head models and validation. Section IV and V discuss and summarize our contributions.

II. MODELS AND METHODS

A. HEAD MODELS

In this study, MRIs of eighteen subjects from the Brian Mutlimodality dataset [44] have been adopted to develop anatomical head models. Two model sets are considered: The first set of models is provided with homogenous dielectric

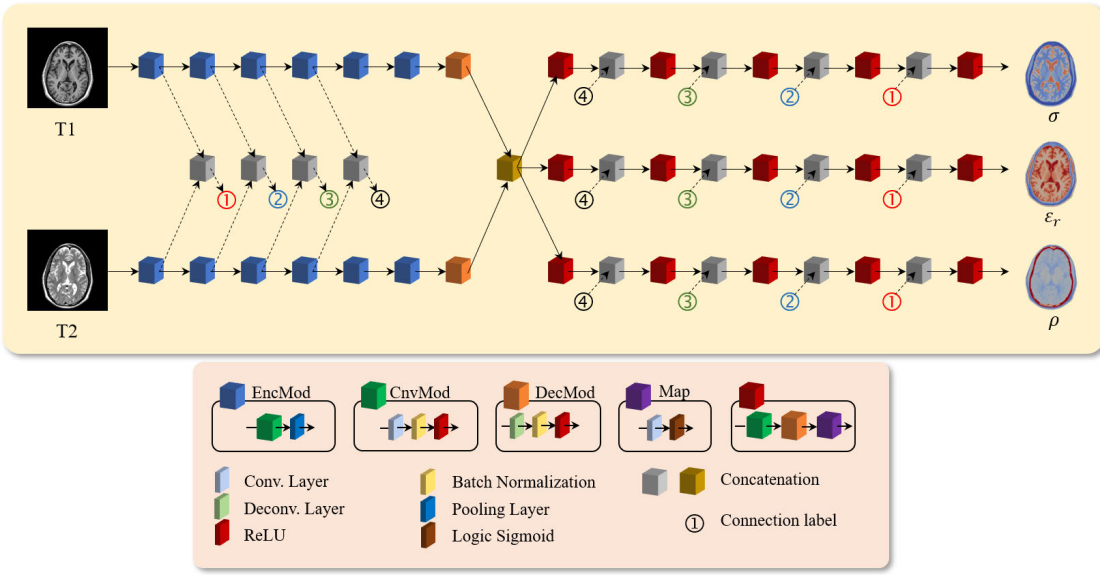

FIGURE 1. The machine learning architecture, CondNet, is used to generate head models in the form of conductivity, relative permittivity, and density matrixes from T1 and T2 MRIs.

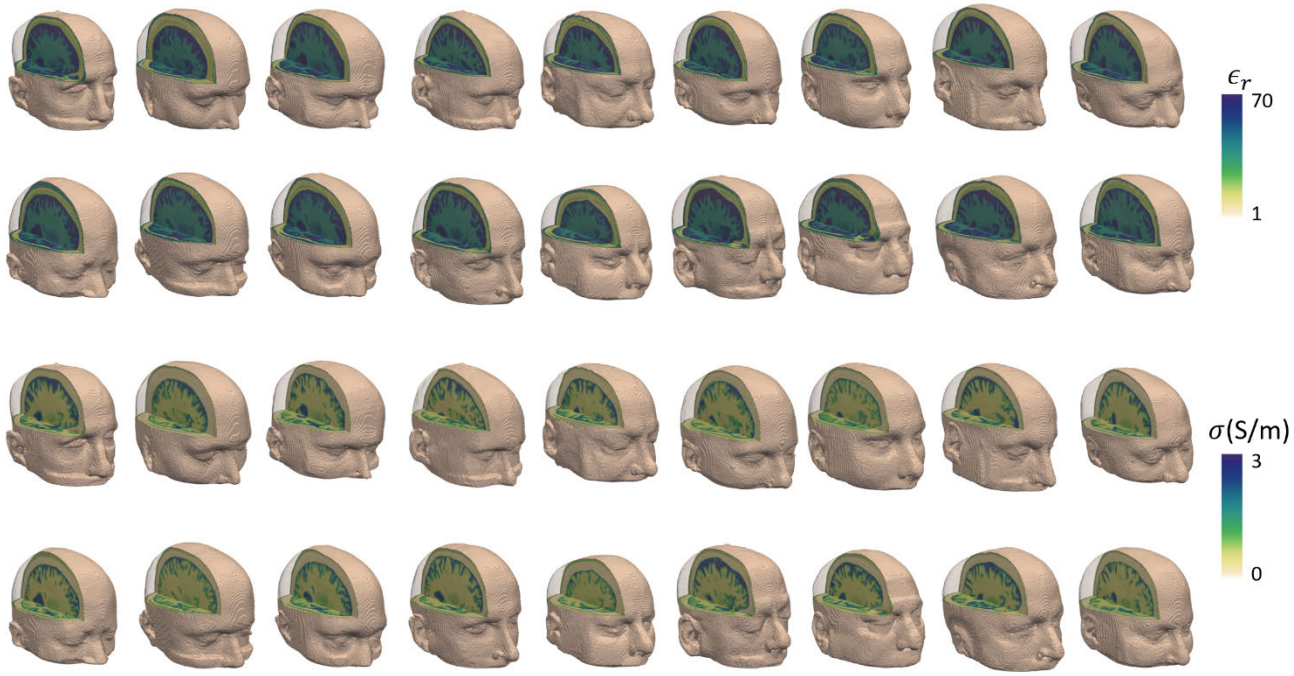

FIGURE 2. Distributions of relative permittivity (top) and conductivity (bottom) of eighteen head models developed from an MRI dataset using a machine learning approach at 0.9 GHz.

properties, which are adopted from [27], as listed in Table 1. Therefore, the difference between each head model lies only in the head shapes. Hereafter, this set of models is referred to as *homogenous heads*.

The second set of head models possesses non-uniformly distributed dielectric properties, which are generated using CondNet [41]. This deep learning architecture (shown in Fig. 1) maps the MRIs to the 3D maps of dielectric properties (σ, ε_r) and tissue density (ρ). The developed learning-based head models are shown in Fig. 2.

CondNet architecture is a multi-track convolutional neural network (CNN) that is designed to estimate dielectric properties and tissue density from anatomical information acquired from an MRI. One potential advantage of CondNet is its ability to estimate physical properties in a smooth pattern that is highly related to the real distribution where sudden

TABLE 1. Dielectric properties of the head tissue equivalent liquid.

Frequency [GHz]	Relative permittivity	Conductivity [S/m]
0.9	41.5	0.97
1.8	40.0	1.4
3.0	38.5	2.4

value change is not common. Moreover, the computational burden of intensive segmentation is not required. Note that conventional voxel models were based on segmentation, and thus the tissue dielectric properties suddenly changed at the tissue boundary, resulting in an abrupt change in the power absorption distribution [41].

In our previous study [41], we have proposed the concept of CondNet for estimation of the non-uniformly distributed dielectric properties and tissue density from MRIs for the first time. However, we only considered the electromagnetic deposition in the exposed heads. The applicability of the learning based models for evaluation of the antenna-body mutual coupling has not been thoroughly examined yet. In addition, the number of models used in that study is not enough to formulate a robust statistical analysis. In this study, by comparisons with homogeneous and segmented models, we demonstrated the applicability of the CondNet models for evaluation of the head proximity effects on antenna radiation performances. More importantly, a large number of head models were developed, making it possible to investigate the inter-subject variations of the head proximity effects in a more appropriate way.

B. ELECTROMAGNETIC SIMULATION CONFIGURATION

The scenarios considered here are a half-wave dipole antenna operated within close vicinity to the human head at 0.9, 1.8, and 3.0 GHz. These frequencies are within the commonly employed bands of several hundred MHz to around 3 GHz for existing mobile communication services. The antenna lengths are 157, 79, and 47 mm, at 0.9, 1.8, and 3.0 GHz, respectively. The feeding point location was 20 mm in front of and 50 mm superior to the right ear canal. The distances between the feeding point and head were 20 and 10 mm, respectively.

In-house software using the FDTD method [43] has been used for electromagnetic analysis. A 15-layer convolutional perfect matched layer (CPML) [45] is used to truncate the simulation domain. The total computation domain consists of $330 \times 330 \times 330$ grids, with a spatial resolution of 1 mm. The antenna parameters, including antenna impedance, RL, directivity, horizontal radiation pattern, TRP, and psSAR were calculated. All results were normalized to a net antenna accepted power of 20 dBm.

III. RESULTS

A. EFFECT OF MODEL SHAPE IN HOMOGENEOUS HEAD MODELS

We first evaluated the antenna parameters using eighteen homogeneous head models as well as SAM phantom. The calculated RLs, directivities, TRPs, and psSARs are listed in Table 2. The mean RLs are higher than 7 dB for all simulated cases, and generally decrease with frequency. The SDs in RL also decrease with increased frequency. The highest SDs are found to be 0.79 dB and 1.46 dB at 0.9 GHz, for distances of 20 and 10 mm, respectively.

The calculated antenna patterns are shown in Fig. 3. In the directions opposite to the human head model, the antenna patterns of the homogeneous heads as well as the SAM phantoms show similar shapes, with slight differences observed in the direction toward the head. As seen in Table 2, the mean values of antenna directivities revealed an increasing trend with the frequency, for example, from 5.4 dBi at 0.9 GHz increasing to 8.09 dBi at 3.0 GHz for the antenna-head distance of 10 mm. The directivity for a half-wave dipole antenna in free space is 2.2 dBi (textbook). In the presence of the head model, the lossy biological medium absorbs the EM power or blocks the EM propagation in the direction toward the head, leading to a higher directivity compared with that in free space. The SDs in the directivities are rather small (<0.4 dB) for all simulated cases.

TABLE 2. Mean and standard deviation of the antenna parameters for the eighteen homogeneous head models.

Dist. [mm]	Freq. [GHz]	RL [dB]			D [dBi]			TRP [mW]			psSAR [W/kg]		
		18 homo heads		SAM	18 homo heads		SAM	18 homo heads		SAM	18 homo heads		SAM
		Mean	SD		Mean	SD		Mean	RSD [a]		Mean	RSD [a]	
20	0.9	10.44	0.79	10.83	5.62	0.20	6.09	35.0	5.6%	41.0	0.53	3.7%	0.47
	1.8	8.71	0.23	9.14	7.57	0.14	7.39	59.7	2.9%	66.3	0.68	2.9%	0.55
	3.0	9.13	0.21	10.07	7.59	0.17	6.92	77.9	1.1%	80.5	0.54	3.3%	0.45
10	0.9	11.79	1.46	12.02	5.40	0.36	5.37	16.9	11.5%	21.6	0.90	2.6%	0.83
	1.8	9.61	0.29	9.00	7.44	0.28	7.39	26.8	9.6%	37.1	1.88	2.0%	1.54
	3.0	7.37	0.17	7.65	8.09	0.21	7.70	49.4	5.1%	59.3	2.16	2.8%	1.60

[a]Relative standard deviations were used for TRP and psSAR.

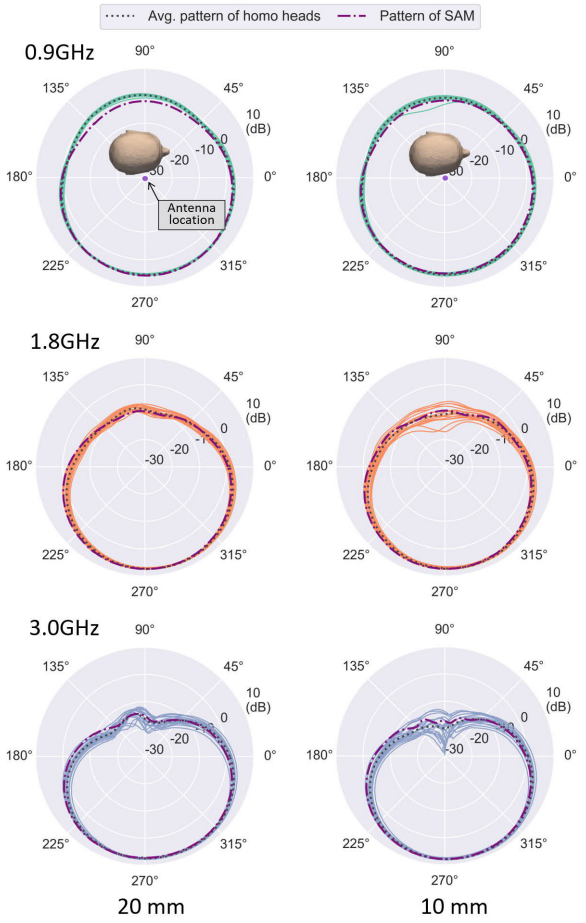

FIGURE 3. Radiation pattern on the horizontal plane for 20 mm (left) and 10 mm (right) distances at frequencies of 0.9 (top), 1.8 (middle) and 3.0 (bottom) GHz. Gray dotted curves represent the averaged patterns of the eighteen homogeneous head models, and purple dash-dotted curves represent the SAM phantom patterns.

The calculated mean TRPs show a steadily increasing trend with frequency, as can be seen in Table 2. The highest mean TRPs are found to be 77.9 mW and 49.4 mW at 3.0 GHz for the 20 and 10 mm distances, respectively. A decreased distance leads to lowered TRPs, indicating that more electromagnetic power is absorbed by the head. The RSD in the TRP declines with frequency. The largest RSD in TRP was found to be 5.6% and 11.5% at 0.9 GHz for the 20 and 10 mm distances, respectively. The mean psSAR also increases with frequency, and smaller distances lead to higher psSAR values. The differences in psSAR among the eighteen homogeneous heads are marginal, the highest RSD in psSAR is found to be 3.7% at 0.9 GHz for a 20 mm distance, and 2.8% at 3.0 GHz for a 10 mm distance. For the antenna parameters listed in Table 2, the largest SDs/RSDs tend to appear at a lower frequency. This is mainly attributable to the longest antenna arm; thus, the geometry variations of the head models in the projection regions of the antenna are the largest.

The SAM phantom results are also listed in Table 2. The largest differences in RLs and directivities between the mean of the eighteen homogeneous heads and SAM phantom are 0.94 dB and 0.67 dB, respectively. The SAM phantom TRPs are higher than the mean homogeneous head values. The psSARs in the SAM phantom were lower than those in the homogenous heads. This is because the SAM phantom contains a low-dielectric plastic shell with a thickness of approximately 2 mm, leading to a slightly larger distance between the antenna and lossy head simulant. If the distance is compensated by moving the SAM toward the antenna by 2 mm, then the differences in TRP and psSAR between homogeneous heads and SAM phantom are decreased.

B. EFFECT OF DIELECTRIC PROPERTIES IN HOMOGENEOUS HEAD MODELS

The dielectric properties of the tissue-equivalent liquid are allowed to have a 20% uncertainty from the targeted σ_t and $\varepsilon_{r,t}$, as listed in Table 1, in accordance with the CTIA test plan [27]. To investigate the effect of the variations of the dielectric properties on the antenna performance, five cases, listed in Table 3, are investigated.

The calculated RLs are shown in Fig. 4 a) for the eight selected head models with varying dielectric properties. The RL variations are generally within 1 dB at 1.8 and 3.0 GHz; slightly larger variations are found at 0.9 GHz. In general, the RLs are higher than 8 dB for most models and cases.

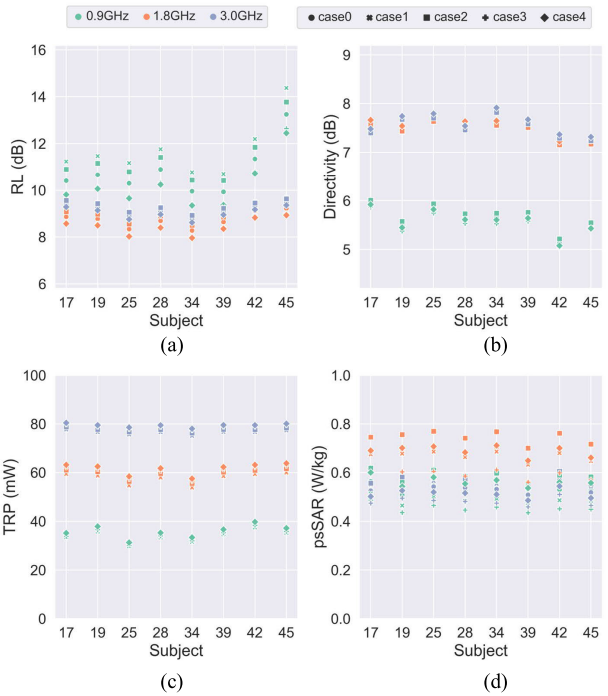

FIGURE 4. Parameters: a) Return loss, b) directivity, c) total radiated power, and d) peak spatial-average SAR for homogeneous head models with varying dielectric properties.

As seen in Fig. 4 b) and c), the directivity and TRP variations caused by the dielectric properties are trivial. Fig. 4 d) and Table 4 show the variations in the psSAR; the largest deviation from Case 0 is 14.8%. As a general rule, psSAR is proportional to tissue conductivity but inversely proportional

TABLE 3. Simulated cases for different dielectric properties of homogeneous heads.

Case No.	Conductivity	Permittivity
0	σ_t	$\varepsilon_{r,t}$
1	$0.8\sigma_t$	$0.8\varepsilon_{r,t}$
2	$0.8\sigma_t$	$1.2\varepsilon_{r,t}$
3	$1.2\sigma_t$	$0.8\varepsilon_{r,t}$
4	$1.2\sigma_t$	$1.2\varepsilon_{r,t}$

to permittivity [13]. This tendency is clearly observed by Case 2 resulting in the highest psSAR and Case 3 resulting in the lowest. In contrast, the deviations of Cases 1 and 4 from Case 0 are marginal. After applying the SAR correction method proposed in [13], the uncertainties in psSAR caused by the variations in dielectric properties are mitigated, as shown in Table 4, and the maximum relative deviations from Case 0 are 4.4%.

TABLE 4. Maximum relative deviations in uncorrected and corrected psSAR from case 0.

Subject	Uncorrected psSAR			Corrected psSAR		
	0.9GHz[a]	1.8GHz[a]	3GHz[a]	0.9GHz[b]	1.8GHz[c]	3GHz[c]
17	13.6%	13.1%	9.7%	4.1%	4.4%	4.2%
19	14.3%	13.2%	9.9%	3.2%	3.9%	3.9%
25	14.8%	13.8%	10.5%	2.5%	4.0%	3.8%
28	14.8%	13.6%	10.4%	2.7%	4.1%	3.7%
34	14.3%	13.2%	10.7%	2.5%	3.8%	3.8%
39	14.0%	13.1%	9.7%	3.8%	4.2%	4.2%
42	14.8%	13.9%	10.3%	2.8%	4.1%	3.9%
45	14.7%	13.4%	10.3%	3.5%	4.4%	4.2%
Mean	14.4%	13.4%	10.2%	3.2%	4.1%	4.0%

[a]Case 3
[b]Case 2
[c]Case 4

The radiation patterns for the five simulated cases of the head model of subject No. 17 are shown in Fig. 5. As seen, uncertainties in the dielectric properties within 20% do not lead to noticeable changes in the antenna radiation patterns.

C. EFFECT OF MODEL INHOMOGENEITY

We then adopted the learning-based head models with inhomogeneous dielectric properties to evaluate the impedance, RL, directivity, pattern, TRP, and psSAR. The results are listed in Table 5. In general, larger SDs and RSDs are found for the learning-based models compared with the homogenous heads. The highest SDs in RL are found to be 1.4 dB and 3.3 dB at 0.9 GHz for 20 and 10 mm distances, respectively. The directivity variances are rather low. The directivity SDs are below 0.2 dB and 0.32 dB for 20 and 10 mm distances,

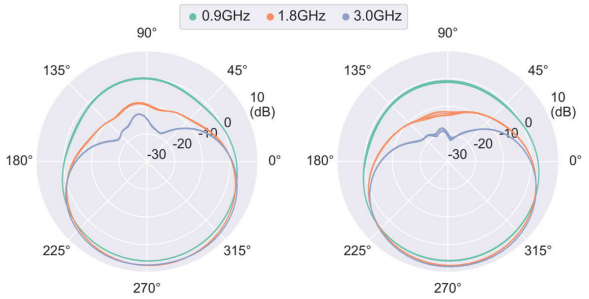

FIGURE 5. Radiation pattern when antennas are placed at a) 20 mm and b) 10 mm from the homogeneous head model of Subject 17 with varying dielectric properties.

TABLE 5. Mean and standard deviation of the antenna parameters for the eighteen learning-based head models.

Freq [GHz]	RL [dB]		D [dBi]		TRP [mW]		psSAR [W/kg]	
	Mean	SD	Mean	SD	Mean	RSD[a]	Mean	RSD[a]
Distance = 20 mm								
0.9	12.9	1.4	5.6	0.19	32.0	5.7%	0.37	7.3%
1.8	9.5	0.7	7.4	0.15	55.3	4.9%	0.56	15%
3.0	9.6	0.6	7.6	0.18	70.9	5.4%	0.59	14%
Distance = 10 mm								
0.9	16.2	3.3	5.5	0.30	16.7	9.2%	0.58	8.0%
1.8	10.7	1.3	7.3	0.32	26.2	9.2%	1.31	8.4%
3.0	9.6	1.2	7.9	0.28	37.2	14%	2.14	6.3%

[a]Relative standard deviations were used for TRP and psSAR.

respectively. The largest RSD in TRP is 14% at 3.0 GHz for a 10 mm distance. The largest RSD in psSAR was found to be 15% at 1.8 GHz for a 20 mm distance. Detailed comparisons between the homogeneous and learning-based head models are shown in Fig. 6–11.

First, we show the impedance dependence with antenna-head distance. The real and imaginary impedance parts for distances from 5 to 50 mm are shown in Fig. 6. As the distance increases, the real impedance part first peaks at approximately 0.3 wavelength (as seen for 3.0 GHz) and then decreases to the free-space impedance (approximately 73 Ω). The imaginary part reaches a maximum at approximately 0.2 wavelength, and then gradually decreases. For a distance of 5 mm, the largest impedance variations are observed. Outliers are found at 0.9 GHz with a distance of <10 mm. This is attributable to the geometrical shape of Subject No. 17, whose right cheek is quite close to the lower tip of the antenna arm at 0.9 GHz. Therefore, distances of less than 5 mm were not considered in this study.

Comparisons of the RL calculated using the learning-based and homogenous head models are shown in Fig. 7. For the 10 mm antenna-head distance, the RL ranges from

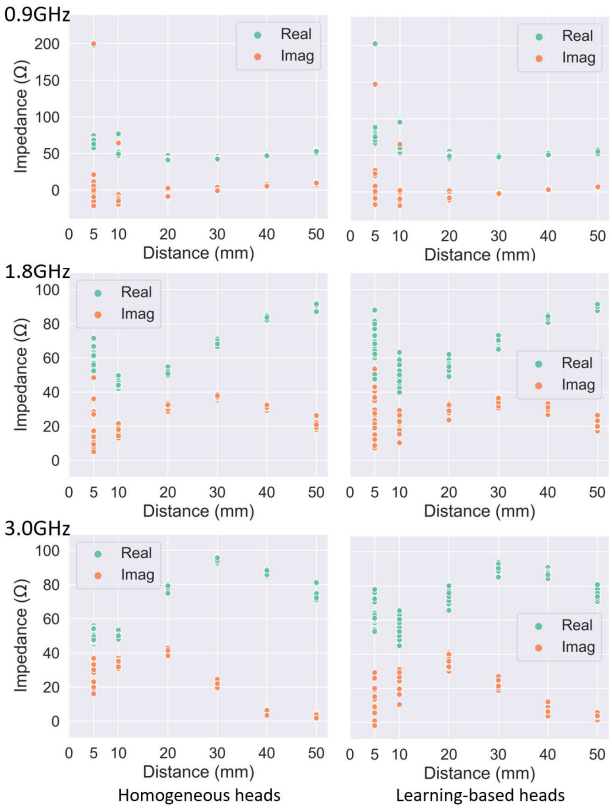

FIGURE 6. Dependence of impedance with distance between antenna and head for homogeneous (left) and learning-based (right) head models at frequencies of 0.9 (top), 1.8 (middle) and 3.0 (bottom) GHz.

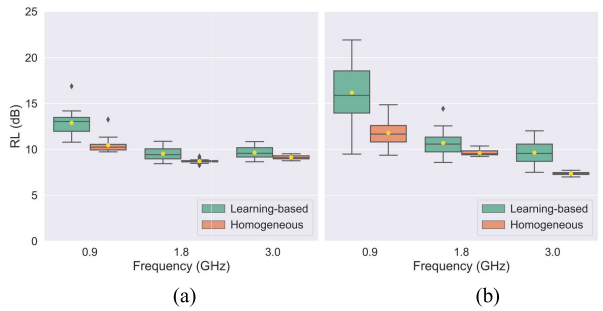

FIGURE 7. Return loss for distances of a) 20 mm and b) 10 mm from the learning-based and homogeneous head models. Yellow dots represent mean values. Homogeneous and learning-based head models were compared to clarify the effect of model inhomogeneity.

approximately 9 to 22 dB at 0.9 GHz, and ranges from 7 to 12 dB at 3 GHz for learning-based heads. Compared to homogeneous heads, wider interquartile ranges are observed for the learning-based models, as expected. In general, the medians are >10 dB at 0.9 GHz and <10 dB at 3.0 GHz.

Homogeneous head models tend to provide poorer (lower) RL values, and a higher frequency results in smaller variations.

Fig. 8 reveals that the differences in directivities between the homogeneous and learning-based head models are marginal. This suggests that the antenna directivity is primarily dependent on the geometry of lossy medium,

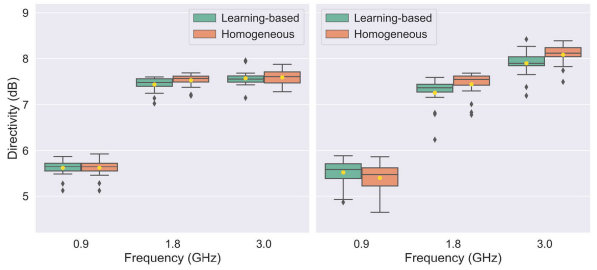

FIGURE 8. Antenna directivities for distances of a) 20 mm and b) 10 mm from the learning-based and homogeneous head models.

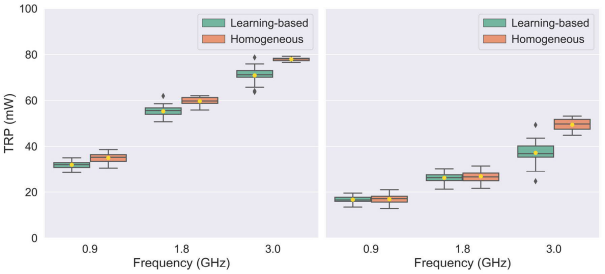

FIGURE 9. Total radiated power for distances of a) 20 mm and b) 10 mm from the learning-based and homogeneous head models.

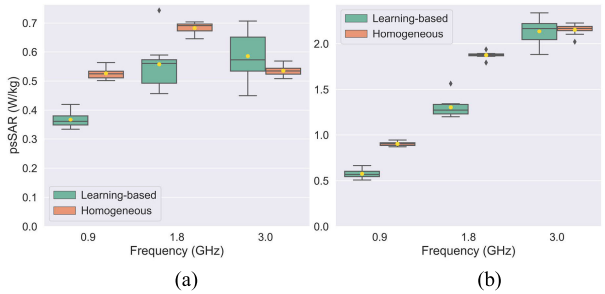

FIGURE 10. Peak spatial-average SAR for distances of a) 20 mm and b) 10 mm from the learning-based and homogeneous head models.

while it is less dependent on the internal dielectric property distribution.

The TRP and psSAR are shown in Fig. 9 and Fig. 10, respectively. As seen, the difference in TRP between homogeneous and learning-based heads increases with frequency. In most cases, the homogenous heads give higher median and mean TRPs. The largest mean TRP difference between homogeneous and learning-based heads is 32.7% at 3.0 GHz for a 10 mm distance. The widths of the TRP interquartile ranges are similar for both sets of models. The differences in psSARs were larger compared to the other parameters. In general, the inter-subject variations in psSAR for learning-based heads are much larger than the homogeneous heads, especially at 3.0 GHz. In most simulated cases, using homogeneous head models leads to more conservative psSARs, the mean psSAR for a homogeneous head is 56.8%

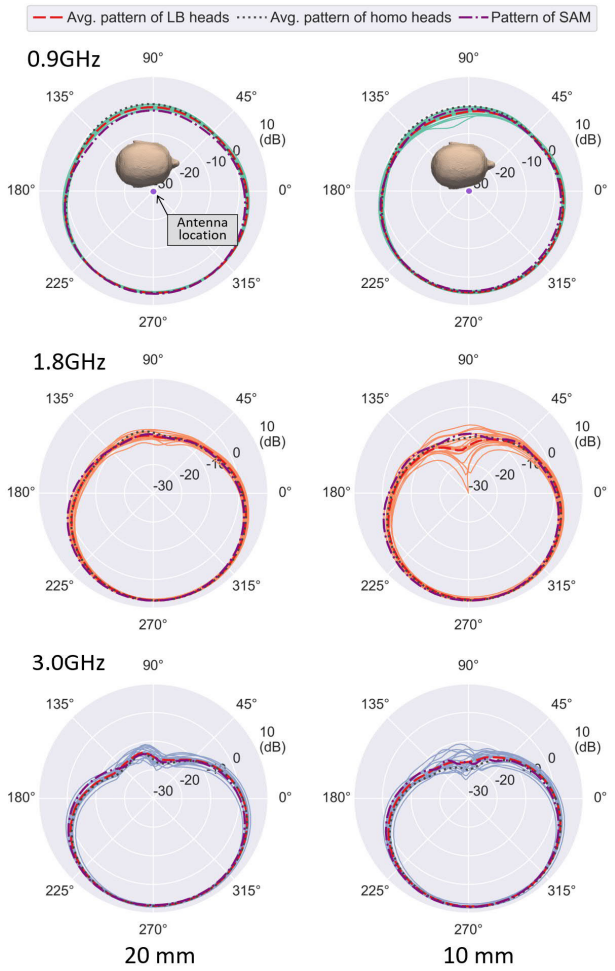

FIGURE 11. Radiation pattern on the horizontal plane for 20 mm (left) and 10 mm (right) distances at frequencies of 0.9 (top), 1.8 (middle) and 3.0 (bottom) GHz. Red dashed and black dotted curves represent the averaged patterns over the eighteen learning-based and homogeneous heads, respectively. Purple dash-dotted curves represent the radiation patterns for the SAM phantom.

higher than that for the learning-based head at 0.9 GHz for a 10 mm distance. However, at 3.0 GHz, the median and mean psSARs of learning-based heads are both higher than those for homogeneous heads. This finding is in line with that reported in [46]. When the distance between the antenna and head is larger than a fraction of wavelength, an increase in the psSAR in an anatomical head can be observed.

The radiation patterns are shown in Fig. 11. As seen, the patterns in the directions opposite to the head models are less affected by the models. Rather large variations in the patterns are found mainly in the directions toward the head for the 10 mm distance at 1.8 and 3.0 GHz.

D. COMPARISON WITH SEGMENTED HEAD MODELS

Historically, voxel-based human models were developed by segmenting anatomical tissues from medical images. The results in [41] reveal that the internal SAR values calculated using the segmented model are more likely to cause staircasing effects because of the hard discontinuity on the tissue interfaces. In contrast, the learning-based head models provide more smoothly distributed dielectric properties, and hence the electromagnetic doses inside the head models are less affected by the staircasing effects around the tissue interfaces.

Comparisons of the antenna parameters between the eight selected learning-based and segmented head models at 1.8 GHz are listed in Table 6. As seen, the largest RL difference is 0.34 dB for Subject 42, and the difference between the mean values is 0.06 dB. Differences in the antenna directivities are all below 0.1 dB. The TRP and psSAR values of the learning-based head models also agree well with those calculated using segmented models.

TABLE 6. Antenna parameters calculated using learning-based (L) and segmented (S) head models at 1.8 GHz for a 20 mm distance.

Subject	RL [dB]		D [dBi]		TRP [mW]		psSAR [W/kg]	
	L	S	L	S	L	S	L	S
17	10.16	10.24	7.52	7.42	54.2	52.1	0.57	0.54
19	8.67	8.55	7.50	7.55	58.6	59.1	0.48	0.49
25	9.55	9.85	7.58	7.54	50.8	50.2	0.56	0.52
28	9.04	9.25	7.44	7.45	55.8	55.2	0.46	0.44
34	8.85	9.17	7.58	7.58	54.6	53.5	0.50	0.48
39	10.62	10.86	7.37	7.32	51.7	51.3	0.59	0.53
42	10.12	9.78	7.14	7.14	57.0	57.9	0.56	0.48
45	10.89	10.70	7.02	6.99	55.4	56.1	0.74	0.73
Mean	9.74	9.80	7.39	7.38	54.8	54.4	0.56	0.53

Comparisons of the antenna radiation patterns on the horizontal plane are shown in Fig. 12. As seen, the patterns are almost identical for the learning-based and segmented heads. The differences in the normalized electric field distributions at time step 10000 for Subject 17 at 1.8 GHz are shown in Fig. 13. Smoother internal electric field distributions are observed for the learning-based models. The field distributions outside the head model in the left-half space for the two models are almost identical, with small differences observed in the right-half space of the simulation space. This also verifies the finding that small pattern variations are only observed in the directions toward the head.

E. VALIDATION

Validation of the calculations was confirmed by comparing antenna parameters with commercial full-wave simulation software XFDTD [47] using the SAM phantom. In the validation, the distance between the antenna and SAM was set to 20 mm, and the CAD-based SAM model was directly imported into XFDTD for discretization. The results for 0.9, 1.8, and 3.0 GHz are listed in Table 7. As seen, the antenna parameters calculated by the in-house program and XFDTD are in good agreement. The largest discrepancies in RLs

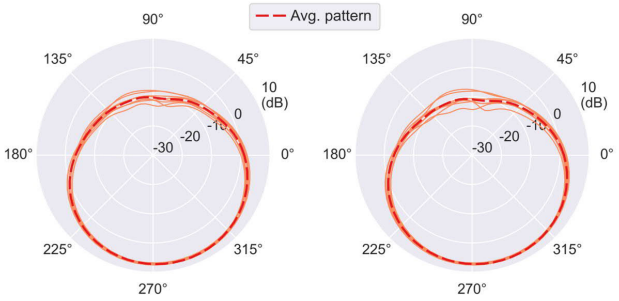

FIGURE 12. Radiation patterns of a) learning-based and b) segmented head models for 20 mm distance.

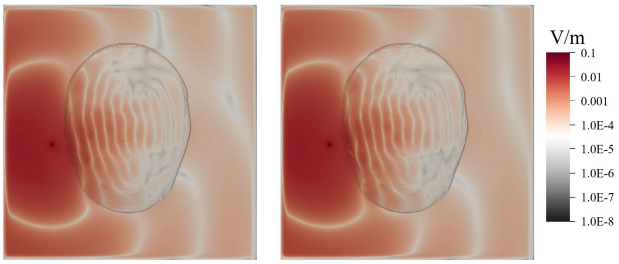

FIGURE 13. Distributions of normalized electric fields on the cross section at time step 10000. Antennas are placed at 20 mm from a) learning-based and b) segmented head models of Subject 17 at 1.8 GHz.

TABLE 7. Comparison of antenna parameters calculated by in-house program (I) and XFDTD (II).

Freq [GHz]	RL [dB]		D [dBi]		TRP [mW]		psSAR [W/kg]	
	I	II	I	II	I	II	I	II
0.9	10.8	11.4	6.09	5.84	41.0	39.2	0.47	0.48
1.8	9.14	8.19	7.39	7.45	66.3	64.0	0.55	0.58
3.0	10.1	10.1	6.92	6.90	80.5	79.9	0.45	0.44

and directivities are 0.95 dB and 0.25 dB, respectively. The relative differences in TRP and psSAR were all below 5.2%. The reason for such slight differences is suspected to be the post-processing methods, the variations in the antenna position [48], and the discretization of the CAD-based models.

IV. DISCUSSION

Recently, machine-learning approaches have been used to develop human models [40], [41]. These approaches differ from the traditional approach of segmenting MRIs to tissues or organs, which inevitably requires the intervention of manual efforts from experienced medical experts [41]. In [41], a few head models were developed and only the SARs in the heads were preliminarily evaluated. In this study, a large number of head models have been developed, making it possible to quantitatively analyze inter-subject variations. The antenna parameters, including RL, directivity, TRP, radiation pattern, and psSAR, were evaluated for the first time using large-scale head models developed by machine learning.

We also investigated the antenna parameters and psSAR using homogenous head models; thus, the uncertainties caused by the homogeneity of the tissue properties and the head geometry can be distinguished. It is shown that using the homogeneous models and SAM phantom with dielectric properties adopted from the CTIA test plan are able to provide acceptable far-field parameter estimations, such as directivity and radiation patterns. The homogeneous heads generally provide a conservative RL estimation, while an optimistic estimation of TRP is observed compared with learning-based heads. However, the discrepancies between homogeneous and learning-based heads are expected to be higher for wearable or implantable wireless devices because of the close contact with the lossy human tissues.

The SDs in directivity and TRP for homogenous and learning-based heads are similar, indicating that these far-field parameters as well as radiation patterns are less likely to be affected by internal tissue distributions. The SDs in RL are higher for learning-based heads than for homogenous heads. The non-uniform dielectric property distributions in learning-based heads contribute to a 1 – 2 dB increase in the SDs in RL for a 10 mm distance (see Tables 2 and 5). Large inter-subject variation in psSAR is also observed for the learning-based heads, compared to the homogeneous ones. The discrepancies in mean psSARs between homogeneous and learning-based models are highly dependent on frequency and antenna locations (see Fig. 10). Therefore, insufficient accuracy in RL and psSAR can be expected when using simplified body models in antenna design, and the subject-specific model is preferred for incorporation in the antenna design phase to minimize the possible parameter deviations from design objectives, especially for personalized applications.

In [32], the SAM phantom conservativeness in the evaluation of psSAR was investigated using nine anatomical head models for mobile phones operated below 2 GHz. Their results revealed that the psSAR evaluated with the SAM phantom can be considered conservative. This tendency is also observed in this study at 0.9 GHz and 1.8 GHz (see Fig. 10). However, at 3.0 GHz, the psSAR assessed using the learning-based heads were higher than those with the homogeneous heads and SAM phantom. This issue requires further investigation, as the frequency bands between 3 and 6 GHz have been allocated for 5G mobile communication.

In addition, the uncertainties of the homogeneous dielectric properties within 20% have little effect on the antenna far-field parameters, such as directivity, TRP, and radiation pattern. Relatively higher variations were found for RL and psSAR due to changes in the dielectric properties of homogeneous heads. One method to overcome this problem is to propose a compensation method with proper correction factors [13]; another is to develop proper dielectric properties for

such human models (homogenous or consists of several major tissues/organs), which is suitable for commercial simulation tools. These issues require further investigation.

Inter-subject variations in the antenna parameters have been previously investigated by measurements. In [5], TRP is evaluated from thirteen subjects when using mobile phones with head proximity, the SDs are approximately 0.8 dB and 0.4 dB at 0.9 GHz and 1.8 GHz, respectively. In the measurements, plastic support was adopted to adjust the mobile phone to a relatively fixed position. When the antenna is held by hand without precise positioning, the SDs increase to approximately 2.7 dB and 2.8 dB, for 0.9 GHz and 1.8 GHz, respectively. Our calculated SDs in TRP using eighteen learning-based head models are about 0.2 dB and 0.4 dB for 20 and 10 mm distances, respectively. Similar SD values were also found for homogenous heads. These values generally agree with the measurement results. The slightly higher SDs in the measured TRPs may be caused by the variation in the mobile phone positions. In addition, the precise distances between the antenna and head are unknown in the measurement using real mobile phones. In our numerical simulations, the antenna location is kept at a fixed location to the head. For portable wireless devices, such as mobile phones, the variability of the human body is small, and relatively large uncertainties are caused by the source location [49].

In this study, the antenna is oriented parallel to the human vertical axis to minimize the effect caused by the neck and shoulder, which are not included in the MRIs. As revealed in [11] and [50], the effects of the neck and shoulder on the antenna performance are insignificant for a vertical dipole antenna if the antenna-head distance is less than approximately 50 mm. The antenna was placed several centimeters from the ear canal in this study. This setting lowers the uncertainty caused by the pinna. The significantly large uncertainties caused by the complex shape of pinna [31] may overwhelm the variation caused by the homogeneity of dielectric property distributions, making it difficult to compare homogenous and learning-based models. In addition, the existing SAR measurement does not include the pinna. In SAM phantom, pinna is constructed as a lossless ear spacer.

V. CONCLUSION

In this study, a total of eighteen anatomical head models were developed using a machine learning approach and then adopted for large-scale evaluation of the inter-subject variations in antenna performance toward personalized wireless devices. Statistical analysis of the antenna impedance, RL, TRP, directivity, radiation pattern, and psSAR were conducted. The computation results show relatively large variations in impedance, RL, and psSAR among different head models, while the internal tissue distributions are less likely to affect the directivity and radiation pattern. Using head models developed by the machine learning approach, robust evaluations of the antenna parameters can be expected to provide comparable results with the traditionally adopted segmented models, significantly reducing the effort of segmenting each tissue/organ. Using head models with homogeneous dielectric properties adopted from the CTIA test plan is acceptable for evaluating antenna far-field parameters, while less accuracy is experienced for RL and psSAR. For frequency bands above 6 GHz for 5G wireless communication, smaller inter-subject variations in antenna parameter can be expected, due to the shallower penetration depth and decreased antenna dimension.

REFERENCES

[1] C. Liu, Y. Guo, S. Xiao, and R. Tmm, "A review of implantable antennas for wireless biomedical devices," *Forum Electromagn. Res. Methods Appl. Technol.*, vol. 14, no. 3, pp. 1–8, 2010.

[2] I.-M. Chen, S. J. Phee, Z. Luo, and C. K. Lim, "Personalized biomedical devices & systems for healthcare applications," *Frontiers Mech. Eng.*, vol. 6, no. 1, pp. 3–12, 2011.

[3] R. Khan, A. A. Al-Hadi, and P. J. Soh, "Recent advancements in user effect mitigation for mobile terminal antennas: A review," *IEEE Trans. Electromagn. Compat.*, vol. 61, no. 1, pp. 279–287, Feb. 2019.

[4] J. O. Nielsen, G. F. Pedersen, K. Olesen, and I. Z. Kovács, "Statistics of measured body loss for mobile phones," *IEEE Trans. Antennas Propag.*, vol. 49, no. 9, pp. 1351–1353, Sep. 2001.

[5] J. Krogerus, J. Toivanen, C. Icheln, and P. Vainikainen, "Effect of the human body on total radiated power and the 3-D radiation pattern of mobile handsets," *IEEE Trans. Instrum. Meas.*, vol. 56, no. 6, pp. 2375–2385, Dec. 2007.

[6] K. Zhao, C. Gustafson, Q. Liao, S. Zhang, T. Bolin, Z. Ying, and S. He, "Channel characteristics and user body effects in an outdoor urban scenario at 15 and 28 GHz," *IEEE Trans. Antennas Propag.*, vol. 65, no. 12, pp. 6534–6548, Dec. 2017.

[7] I. Syrytsin, S. Zhang, G. F. Pedersen, K. Zhao, T. Bolin, and Z. Ying, "Statistical investigation of the user effects on mobile terminal antennas for 5G applications," *IEEE Trans. Antennas Propag.*, vol. 65, no. 12, pp. 6596–6605, Dec. 2017.

[8] I. Syrytsin, S. Zhang, and G. F. Pedersen, "User impact on phased and switch diversity arrays in 5G mobile terminals," *IEEE Access*, vol. 6, pp. 1616–1623, Dec. 2018.

[9] D. Naranjo-Hernández, J. Reina-Tosina, and L. M. Roa, "Lessons learned about the design and active characterization of on-body antennas in the 2.4 GHz frequency band," *Sensors*, vol. 20, no. 1, p. 224, Dec. 2019.

[10] M. A. Jensen and Y. Rahmat-Samii, "EM interaction of handset antennas and a human in personal communications," *Proc. IEEE*, vol. 83, no. 1, pp. 7–17, Jan. 1995.

[11] K. Ogawa, T. Matsuyoshi, and K. Monma, "A study of the effects of the shoulder on the effective gain characteristics in the multiple radio wave environment of a dipole antenna close to a human head," *Electron. Commun. Jpn. I, Commun.*, vol. 84, no. 1, pp. 21–30, Jan. 2001.

[12] R. Takei, T. Nagaoka, K. Saito, S. Watanabe, and M. Takahashi, "SAR variation due to exposure from a smartphone held at various positions near the torso," *IEEE Trans. Electromagn. Compat.*, vol. 59, no. 2, pp. 747–753, Apr. 2017.

[13] M. G. Douglas, M. Y. Kanda, W. G. Luengas, M. Ballen, T. M. Babij, and C.-K. Chou, "An algorithm for predicting the change in SAR in a human phantom due to deviations in its complex permittivity," *IEEE Trans. Electromagn. Compat.*, vol. 51, no. 2, pp. 217–226, May 2009.

[14] G. Bit-Babik, A. Faraone, M. Ballen, and C. K. Chou, "Sensitivity of the spatial-average peak SAR to the dielectric parameters of media used for compliance testing in the frequency range 0.3–3 GHz," in *Proc. IEEE Antennas Propag. Soc. Int. Symp.*, San Antonio, TX, USA, Jun. 2002, pp. 722–725.

[15] J. Ilvonen, O. Kivekäs, J. Holopainen, R. Valkonen, K. Rasilainen, and P. Vainikainen, "Mobile terminal antenna performance with the User's hand: Effect of antenna dimensioning and location," *IEEE Antennas Wireless Propag. Lett.*, vol. 10, pp. 772–775, Jul. 2011.

[16] M. Pelosi, O. Franek, M. B. Knudsen, G. F. Pedersen, and J. B. Andersen, "Antenna proximity effects for talk and data modes in mobile phones," *IEEE Antennas Propag. Mag.*, vol. 52, no. 3, pp. 15–27, Jun. 2010.

[17] T. Nagaoka, S. Watanabe, K. Sakurai, E. Kunieda, S. Watanabe, M. Taki, and Y. Yamanaka, "Development of realistic high-resolution whole-body voxel models of Japanese adult males and females of average height and weight, and application of models to radio-frequency electromagnetic-field dosimetry," *Phys. Med. Biol.*, vol. 49, no. 1, pp. 1–15, Jan. 2004.

[18] M.-C. Gosselin, E. Neufeld1, H. Moser, E. Huber, S. Farcito, L. Gerber, M. Jedensjö, I. Hilber, F. Di Gennaro, B. Lloyd, E. Cherubini, D. Szczerba, W. Kainz, and N. Kuster, "Development of a new generation of high-resolution anatomical models for medical device evaluation: The virtual population 3.0," *Phys. Med. Biol.*, vol. 59, no. 18, p. 5287, Aug. 2014.

[19] P. J. Dimbylow, "FDTD calculations of the whole-body averaged SAR in an anatomically realistic voxel model of the human body from 1 MHz to 1 GHz," *Phys. Med. Biol.*, vol. 42, no. 3, pp. 479–490, Mar. 1997.

[20] P. Dimbylow, "Development of the female voxel phantom, NAOMI, and its application to calculations of induced current densities and electric fields from applied low frequency magnetic and electric fields," *Phys. Med. Biol.*, vol. 50, no. 6, p. 1047, Feb. 2005.

[21] E. A. Rashed, J. Gomez-Tames, and A. Hirata, "End-to-end semantic segmentation of personalized deep brain structures for non-invasive brain stimulation," *Neural Netw.*, vol. 125, pp. 233–244, May 2020.

[22] W. Liu, H. Wang, P. Zhang, C. Li, J. Sun, Z. Chen, S. Xing, P. Liang, and T. Wu, "Statistical evaluation of radiofrequency exposure during magnetic resonant imaging: Application of whole-body individual human model and body motion in the coil," *Int. J. Environ. Res. Public Health*, vol. 16, no. 6, p. 1069, Mar. 2019.

[23] A. Peyman, C. Gabriel, E. H. Grant, G. Vermeeren, and L. Martens, "Variation of the dielectric properties of tissues with age: The effect on the values of SAR in children when exposed to walkie–talkie devices," *Phys. Med. Biol.*, vol. 54, no. 2, pp. 227–241, Dec. 2008.

[24] International Commission on Non-Ionizing Radiation Protection, "Guidelines for limiting exposure to electromagnetic fields (100 kHz to 300 GHz)," *Health Phys.*, vol. 118, no. 5, pp. 483–524, May 2020.

[25] *IEEE Standard for Safety Levels with Respect to Human Exposure to Electric, Magnetic and Electromagnetic Fields, 0 Hz to 300 GHz*, IEEE Standard C95.1, 2019.

[26] *Human Exposure to Radio Frequency Fields From Hand-Held and Body-Mounted Wireless Communication Devices—Human Models, Instrumentation, and Procedures—Part 1*, IEC Standard 62209-1, 2006.

[27] *Test Plan for Wireless Device Over-the-Air Performance*, CTIA Program, Washington, DC, USA, 2018.

[28] N. Kuster, V. Santomaa, and A. Drossos, "The dependence of electromagnetic energy absorption upon human head tissue composition in the frequency range of 300–3000 MHz," *IEEE Trans. Microw. Theory Techn.*, vol. 48, no. 11, pp. 1988–1995, Nov. 2000.

[29] A.-K. Lee and J. Yun, "A comparison of specific absorption rates in SAM phantom and child head models at 835 and 1900 MHz," *IEEE Trans. Electromagn. Compat.*, vol. 53, no. 3, pp. 619–627, Aug. 2011.

[30] C. J. Panagamuwa, W. G. Whittow, R. M. Edwards, and J. C. Vardaxoglou, "Experimental verification of a modified specific anthropomorphic mannequin (SAM) head used for SAR measurements," in *Proc. Loughborough Antennas Propag. Conf.*, Loughborough, Apr. 2007, pp. 261–264.

[31] W. Kainz, A. Christ, T. Kellom, S. Seidman, N. Nikoloski, B. Beard, and N. Kuster, "Dosimetric comparison of the specific anthropomorphic mannequin (SAM) to 14 anatomical head models using a novel definition for the mobile phone positioning," *Phys. Med. Biol.*, vol. 50, no. 14, pp. 3423–3445, Jul. 2005.

[32] J. Keshvari, M. Kivento, A. Christ, and G. Bit-Babik, "Large scale study on the variation of RF energy absorption in the head & brain regions of adults and children and evaluation of the SAM phantom conservativeness," *Phys. Med. Biol.*, vol. 61, no. 8, pp. 2991–3008, Mar. 2016.

[33] M. Okoniewski and M. A. Stuchly, "A study of the handset antenna and human body interaction," *IEEE Trans. Microw. Theory Techn.*, vol. 44, no. 10, pp. 1855–1864, Oct. 1996.

[34] L. C. Fung, S. W. Leung, and K. H. Chan, "Experimental study of SAR reduction on commercial products and shielding materials in mobile phone applications," *Microw. Opt. Technol. Lett.*, vol. 36, no. 6, pp. 419–422, Feb. 2003.

[35] J.-N. Hwang and F.-C. Chen, "Reduction of the peak SAR in the human head with metamaterials," *IEEE Trans. Antennas Propag.*, vol. 54, no. 12, pp. 3763–3770, Dec. 2006.

[36] R. Ikeuchi and A. Hirata, "Dipole antenna above EBG substrate for local SAR reduction," *IEEE Antennas Wireless Propag. Lett.*, vol. 10, pp. 904–906, Sep. 2011.

[37] M. R. I. Faruque, M. T. Islam, and N. Misran, "Design analysis of new metamaterial for EM absorption reduction," *Prog. Electromagn. Res.*, vol. 124, pp. 119–135, Jan. 2012.

[38] N. Hampe, M. Herrmann, T. Amthor, C. Findeklee, M. Doneva, and U. Katscher, "Dictionary-based electric properties tomography," *Magn. Reson. Med.*, vol. 81, no. 1, pp. 342–349, Jan. 2019.

[39] J. E. C. Serralles, R. Lattanzi, I. I. Giannakopoulos, B. Zhang, C. Ianniello, M. A. Cloos, A. G. Polimeridis, J. K. White, D. K. Sodickson, and L. Daniel, "Noninvasive estimation of electrical properties from magnetic resonance measurements via global Maxwell tomography and match regularization," *IEEE Trans. Biomed. Eng.*, vol. 67, no. 1, pp. 3–15, Jan. 2020.

[40] E. A. Rashed, J. Gomez-Tames, and A. Hirata, "Deep learning-based development of personalized human head model with non-uniform conductivity for brain stimulation," *IEEE Trans. Med. Imag.*, vol. 39, no. 7, pp. 2351–2362, Jul. 2020.

[41] E. A. Rashed, Y. Diao, and A. Hirata, "Learning-based estimation of dielectric properties and tissue density in head models for personalized radio-frequency dosimetry," *Phys. Med. Biol.*, vol. 65, no. 6, Mar. 2020, Art. no. 065001.

[42] M. W. Krueger, G. Seemann, K. Rhode, D. U. J. Keller, C. Schilling, A. Arujuna, J. Gill, M. D. O'Neill, R. Razavi, and O. Dossel, "Personalization of atrial anatomy and electrophysiology as a basis for clinical modeling of radio-frequency ablation of atrial fibrillation," *IEEE Trans. Med. Imag.*, vol. 32, no. 1, pp. 73–84, Jan. 2013.

[43] A. Taflove and S. C. Hagness, *Computational Electrodynamics: The Finite-Difference Time-Domain Method*, 3rd ed. Norwood, MA, USA: Artech House, 2005.

[44] *MIDAS—Collection NAMIC: Brain Mutlimodality*. Accessed: Apr. 22, 2020. [Online]. Available: http://insight-journal.org/midas/collection/view/190

[45] J. A. Roden and S. D. Gedney, "Convolutional PML (CPML): An efficient FDTD implementation of the CFS-PML for arbitrary media," *Microw. Opt. Technol. Lett.*, vol. 27, no. 5, pp. 334–338, Oct. 2000.

[46] A. Christ, A. Klingenbock, T. Samaras, C. Goiceanu, and N. Kuster, "The dependence of electromagnetic far-field absorption on body tissue composition in the frequency range from 300 MHz to 6 GHz," *IEEE Trans. Microw. Theory Techn.*, vol. 54, no. 5, pp. 2188–2195, May 2006.

[47] *REMCOM, XFDTD*. Accessed: Apr. 22, 2020. [Online]. Available: https://www.remcom.com/xfdtd-3d-em-simulation-software

[48] B. B. Beard, W. Kainz, T. Onishi, T. Iyama, S. Watanabe, O. Fujiwara, J. Wang, G. Bit-Babik, A. Faraone, J. Wiart, A. Christ, N. Kuster, A.-K. Lee, H. Kroeze, M. Siegbahn, J. Keshvari, H. Abrishamkar, W. Simon, D. Manteuffel, and N. Nikoloski, "Comparisons of computed mobile phone induced SAR in the SAM phantom to that in anatomically correct models of the human head," *IEEE Trans. Electromagn. Compat.*, vol. 48, no. 2, pp. 397–407, May 2006.

[49] E. Reusens, W. Joseph, B. Latre, B. Braem, G. Vermeeren, E. Tanghe, L. Martens, I. Moerman, and C. Blondia, "Characterization of on-body communication channel and energy efficient topology design for wireless body area networks," *IEEE Trans. Inf. Technol. Biomed.*, vol. 13, no. 6, pp. 933–945, Nov. 2009.

[50] E. Ofli, N. Chavannes, and N. Kuster, "The uncertainties and repeatability limitations of transmitter and receiver performance assessments posed by head phantoms," in *Proc. IEEE Int. Workshop Antenna Technol. Small Antennas Novel Metamater.*, New York, NY, USA, Mar. 2006, pp. 349–352.

YINLIANG DIAO (Member, IEEE) received the B.E. degree from Chongqing University, Chongqing, China, in 2008, the M.S. degree in electronic engineering from the Beijing University of Posts and Telecommunications, Beijing, China, in 2011, and the Ph.D. degree in electronic engineering from the City University of Hong Kong, in 2016. Since 2017, he has been an Assistant Professor with South China Agricultural University, Guangzhou, China. In 2019, he joined the Department of Electrical and Mechanical Engineering, Nagoya Institute of Technology, as a Researcher. His current research interests include electromagnetic dosimetry modeling and electromagnetic compatibility.

ESSAM A. RASHED (Senior Member, IEEE) received the B.Sc. degree in scientific computing and the M.Sc. degree in computer science from Suez Canal University, Ismailia, Egypt, in 1998 and 2002, respectively, and the Ph.D. degree in computer science from the University of Tsukuba, Tsukuba, Japan, in 2010. From 2010 to 2012, he was a Research Fellow of the Japan Society for the Promotion of Science (JSPS), University of Tsukuba. He has served as an Assistant Professor with the Department of Mathematics, Faculty of Science, Suez Canal University, Egypt, from 2012 to 2016. Since then, he has been promoted to an Associate Professor with Suez Canal University and The British University in Egypt (on Secondment). He is currently a Research Associate Professor with the Nagoya Institute of Technology. His research interest is medical image processing, data analysis and visualization, deep learning, and pattern recognition. He is an Associate Editor of IEEE ACCESS. He was a recipient of the Egyptian National Doctoral Scholarship in 2006, the JSPS Postdoctoral Fellowship in 2010, the JAMIT Best Presentation Award in 2008 and 2012, and the Chairman Award, Department of Computer Science, University of Tsukuba, in 2010. He has served as a PI for several projects funded from Science and Technology Development Fund (STDF), Egypt.

AKIMASA HIRATA (Fellow, IEEE) received the B.E., M.E., and Ph.D. degree in communications engineering from Osaka University, Suita, Japan, in 1996, 1998, and 2000, respectively.

From 1999 to 2001, he was a Research Fellow of the Japan Society for the Promotion of Science, and also a Visiting Research Scientist with the University of Victoria, Victoria, BC, Canada, in 2000. In 2001, he joined the Department of Communications Engineering, Osaka University, as an Assistant Professor. In 2004, he joined as an Associate Professor with the Department of Computer Science and Engineering, Nagoya Institute of Technology, where he is currently a Full Professor. His research interests include electromagnetic safety, risk management system for heat-related illness, methods in neuroscience, antennas, filters, and related computational techniques.

Prof. Hirata is a Fellow of the Institute of Physics and IEICE, and a member of IEE Japan and Bioelectromagnetics Society. He received several awards including Young scientists' Prize in 2006 and Prizes for Science and Technology (Research Category 2011, Public Understanding Promotion Category 2014) by the Commendation for Science and Technology by the Minister of Education, Culture, Sports, Science, and Technology, Japan, and the IEEE EMC-S Technical Achievement Award in 2015, and the Japan Academy Medal and JSPS Prize in 2018. He is an Editorial Board Member of physics in medicine and biology, a member of the main commission and the Chair of the Project Group of International Commission on Non-Ionizing Radiation Protection, and a member of administrative committee and a Subcommittee (EMF Dosimetry Modeling) Chair of the IEEE International Committee on Electromagnetic Safety, and an expert of World Health Organization. From 2006 to 2012, he was also an Associate Editor of the IEEE TRANSACTIONS ON BIOMEDICAL ENGINEERING.